International Journal of Heat and Mass Transfer 55 (2012) 3900–3908

Contents lists available at SciVerse ScienceDirect

International Journal of Heat and Mass Transfer

journal homepage: www.elsevier.com/locate/ijhmt

Creeping flow through ordered arrays of micro-cylinders embedded in a rectangular minichannel

A. Tamayol *, A. Khosla, B.L. Gray, M. Bahrami

School of Engineering Science, Simon Fraser University, BC, Canada

ARTICLE INFO

Article history:
Available online 3 May 2012

Keywords:
Mini/microchannels filled with porous media
Porous media
Pressure drop
Brinkman equation

ABSTRACT

The pressure drop in microfluidic minichannels filled with porous media formed by square arrays of microcylinders is investigated. We investigate the problem by combining the Brinkman equation and existing models for permeability of regular arrays of cylinders to calculate the pressure drop of the studied geometries theoretically. In order to verify our theoretical analysis, a soft lithography method is employed to fabricate several Polydimethylsiloxane (PDMS) samples with porosities in the range of 0.35 to 0.95, fiber diameters varying from 50 to 400 μm, and channel depth of approximately 100 μm. Distilled water is pushed through the samples using a syringe pump with several steady flow rates and the resulting pressure drops are measured. Moreover, flow through the fabricated samples is solved numerically and the pressure drops are determined. The theoretical model shows a reasonable agreement with experimental and numerical data for all of the tested samples. Our analysis indicates that the geometrical parameters that control the pressure drop are the porous medium permeability and the channel dimensions. Furthermore, the Darcy number can be used to determine the dominating parameter.

1. Introduction

Microchannels offer high heat and mass transfer coefficients, high surface to volume ratio, and low thermal resistance. As such, they have been utilized in applications such as electronics cooling, aerospace, MEMS, medical and biomedical devices [1–4]. The major drawback in using microfluidic chips is the high pressure drop which is a result of their small cross-sectional length scale [5]. To alleviate this problem, the channels cross-sectional size should be increased which reduces the surface to volume ratio of the designed chip. However, one solution is to combine mini/microchannels with porous media to develop a novel design whereby the mini/microchannels are filled with porous media. Similar to microchannels, highly porous structures feature low-weight, high surface-to-volume ratio, and high heat transfer coefficient [6]. Therefore, it is expected that microchannels filled with porous media offer thermal properties similar to that of regular microchannels at the expense of a lower pressure drop.

Microchannels filled with porous media also have potential applications in filtration, detection of particles, controlling surface wettability of microsystems, chromatographic separation, and tissue engineering [7–9]. Moreover such structures have been used in biological and life sciences for analyzing biological materials such as proteins, DNA, cells, embryos, and chemical reagents [10,11].

Although the fully developed and developing flows in channels of various cross-sections filled with porous media have been extensively studied in the literature (see for example [12–14]); such studies for small-scale mini- and micro-size channels are not numerous. Hooman [15,16] have investigated rarefied gas flows in microchannels filled with porous media. However, their theoretical analyses were not verified by any experimental data. Scales and Tait [17] solved volume averaged equations for pressure driven and electroosmotic flows through porous microfluidic devices and reported a sophisticated solution for flow between parallel plates.

Few experimental and numerical studies have been conducted to study the flow through mini/microchannels filled with micro pin fins. Kosar et al. [18] studied laminar flow across four different arrays of micro pin fins embedded inside in microchannels with 100 μm depth. The pin fin diameters employed in their study were 50 and 100 μm. They compared their results for Reynolds numbers in the range of 5–128 with existing correlations for relatively high Reynolds number flows through macro-scale tube banks and observed a significant deviation. Kosar et al. [18] related this deviation to the difference between flow in micron-size systems and geometries where the smallest length scale is larger than 1 mm. Vanapalli et al. [19] measured the pressure drop in microchannels of 250 μm depth containing various pillar arrays in the Reynolds number range of 50–500. On the contrary, their results

* Corresponding author. Address: School of Engineering Science, Simon Fraser University, Laboratory for Alternative Energy Conversion (LAEC), #4300, 250 – 13450 102nd Avenue, Surrey, BC, Canada V3T0A3. Tel.: +1 778 782 8587.
E-mail address: ali_tamayol@sfu.ca (A. Tamayol).

0017-9310/$ - see front matter © 2012 Elsevier Ltd. All rights reserved.
http://dx.doi.org/10.1016/j.ijheatmasstransfer.2012.03.008

Nomenclature

Da	Darcy number ($Da = K/h^2$)
d	cylinder diameter (m)
$E(\cdot)$	uncertainty associated with parameters
h	channel depth (m)
K	permeability (m^2)
L	channel length (m)
m	parameter used in Eq. (3)
P	pressure (N/m^2)
Q	volumetric flow rate (μl/min)
Re	Reynolds number
S	distance between centers of adjacent cylinders (m)
U	volume averaged velocity (m/s)

Greek symbols

φ'	parameter used in Eq. (8)
ε	porosity
ε'	parameter used in Eq. (3)
η	non-dimensional coordinate
μ	viscosity ($N\,s/m^2$)
μ_{eff}	effective viscosity ($N\,s/m^2$)
μ'	viscosity ratio ($\mu' = \mu_{eff}/\mu$)

Subscripts

c	related to connections
D	developing
FD	fully developed
minor	minor losses
ev	electro viscous

for circular pillars were in good agreement with conventional relationships. Yeom et al. [20] reported low Reynolds number flow pressure drops through microchannels filled with arrays of micro-posts with various fibers in square arrangements. The channels were 200 μm deep and the diameters of the micro-posts ranged from 200 μm to less than 10 μm. Similar to [19], they did not include wall effects into their analysis. Therefore, their results for high permeability arrays deviated from the values predicted by conventional theories. Gamarat et al. [21] employed volume averaged equations to study flow through channels partially filled with micro-posts in an attempt to investigate effects of wall roughness on the flow field and pressure drop. They also performed experimental investigations and successfully compared their theoretical analysis with the experimental data.

To the best knowledge of the authors, there has been no study on the pressure drop in microchannels filled with porous media and comparison of the data with the theories developed for macro size geometries (with hydraulic diameters larger than one millimeter). As such, the goals of this study are to:

- Employ the theoretical studies developed for regular size channels for predicting the pressure drop of liquid flows through minichannels filled with porous media.
- Perform independent experimental and numerical studies to verify the theoretical analysis.
- Determine the importance of different parameters such as permeability and cross-sectional length scale on the pressure drop in the investigated geometries.

The focus will be on porous media formed by square arrangements of cylinders. Employing the Brinkman model for confined porous media and the analytical model developed by Tamayol and Bahrami [22] for permeability of square arrangement of fibers, a compact model for estimating pressure drop of ordered arrays of short cylinders embedded in a channel is proposed. In addition, an experimental study is conducted in which water flow pressure drops are measured in several PDMS samples with different cylinder sizes and porosities. Moreover, creeping flow through the fabricated structures is solved numerically to provide a more accurate mean for verifying the theoretical approach.

Through comparison of the proposed model with the experimental and numerical data, it is shown that despite its simplicity, the presented approach is practical and accurate enough for design and optimization purposes in microfluidics.

2. Theoretical background

The microchannel filled with porous media, shown in Fig. 1, is comprised of repeating square arrangements of mono disperse cylinders, embedded in a rectangular microchannel. Several researchers have stated that in the creeping flow regime, the fully developed condition is achieved within the first three rows of cylinders; see for example [23]. Therefore, the entrance effects are neglected in this study. As such, fully developed, steady state, incompressible, and creeping flows of a Newtonian fluid inside the aforementioned geometries are studied.

In low Reynolds number flows in porous media, a linear relationship is assumed between the applied pressure drop and the volume averaged (superficial) velocity which is called the Darcy equation:

$$-\frac{dP}{dx} = \frac{\mu}{K}U \tag{1}$$

where μ is the fluid viscosity and K is the permeability of the medium. The Darcy relationship is empirical, convenient, and widely accepted. However, in applications where a porous material is confined by solid walls, e.g., mini/microchannels filled with porous media, or when the flow inside the porous medium is boundary driven, the Brinkman equation [24] should be used instead:

$$-\frac{dP}{dx} = \frac{\mu}{K}U + \mu_{eff}\frac{d^2U}{dy^2} \tag{2}$$

where μ_{eff} is called the effective viscosity. Previous studies have shown that the viscosity ratio $\mu' = \mu/\mu_{eff}$, varies between 1 to 10 [25]. Some researchers has postulated that $\mu' = 1$; see for example [26] which is a reasonable assumption for highly porous materials [27]. However, Ochoa-Tapia and Whitaker [28] argued that $\mu' = 1/\varepsilon$ is a more accurate assumption; ε is the porosity of the porous medium.

The last term in the right hand side of Eq. (2) has been originally added to the Darcy equation to enable the solution to fulfill the no-slip boundary condition on solid walls. In the limiting case, where either there is no porous medium inside the channel or the boundary effects are dominant, Darcy term, the first term in the right hand side of Eq. (2), vanishes and this equation becomes identical to Stokes equation. On the other hand, in the limit of very dense

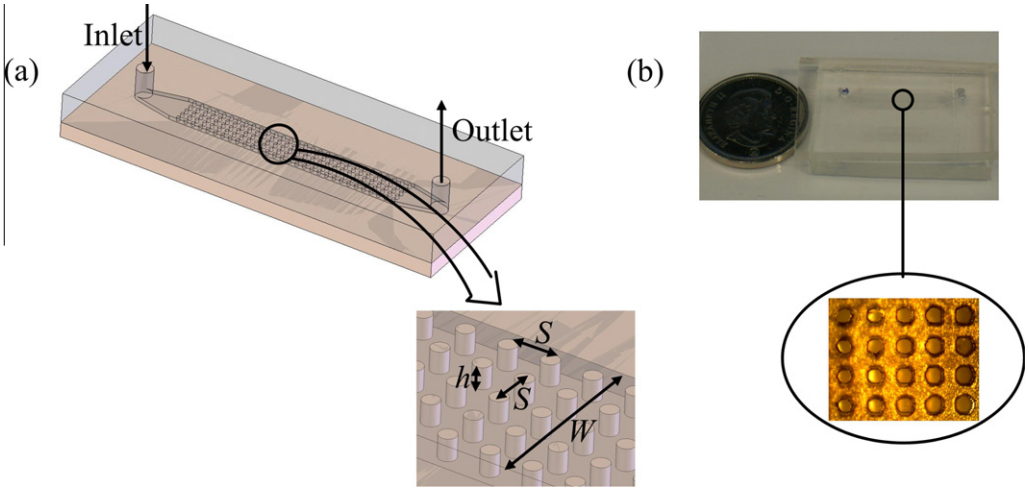

Fig. 1. Structure of the considered porous-filled channels (a) the schematic, (b) a fabricated sample.

porous media, the Darcy term becomes dominant and Eq. (2) reduces to Eq. (1).

Hooman and Merrikh [29] have developed analytical solutions for flow and pressure drop inside large scale rectangular channels filled with porous media:

$$-\frac{\Delta P}{L}=\frac{\mu}{Wh^3}\frac{1}{2\sum_{n=1}^{\infty}\frac{1}{\lambda_n^2 m^2}\left(1-\frac{\tanh m\varepsilon'}{m\varepsilon'}\right)} \tag{3}$$

where,

$$\varepsilon'=\frac{h}{W},\ \lambda_n=\frac{(2n-1)\pi}{2},\ \sqrt{Da^{-1}}=\frac{h}{\sqrt{K}},\ m=\left(\lambda_n^2+Da^{-1}\right)^{1/2} \tag{4}$$

and h, L and W are the depth, length, and width of the channel, respectively. They also assumed that $\mu'=1$. The cross-sectional aspect ratio, $\varepsilon'=h/W$, in the samples tested in the present study is smaller than 0.1. Therefore, instead of considering the whole rectangular cross-section, the sample can be envisioned as a porous medium sandwiched between two parallel plates, as shown in Fig. 2. The solution of Eq. (2), the volume averaged velocity distribution, for 2D flow between parallel plates subject to no-slip boundary condition on the wall becomes:

$$U=\frac{K}{\mu}\frac{dP}{dx}\left[\frac{\sinh\left(\frac{y}{\sqrt{\mu' K}}\right)-\sinh\left(\frac{y-h}{\sqrt{\mu' K}}\right)}{\sinh\left(\frac{h}{\sqrt{\mu' K}}\right)}-1\right] \tag{5}$$

Consequently, the pressure drop for the simplified geometry becomes:

$$-\frac{\Delta P}{L}=\frac{\mu Q\sinh\left(\frac{h}{\sqrt{\mu' K}}\right)}{Kh\left[2\frac{\sqrt{\mu' K}}{h}\left[-1+\cosh\left(\frac{h}{\sqrt{\mu' K}}\right)\right]-\sinh\left(\frac{h}{\sqrt{\mu' K}}\right)\right]} \tag{6}$$

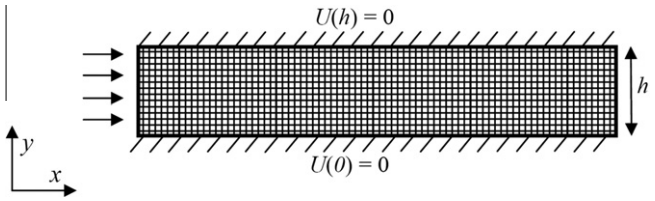

Fig. 2. Schematic of the simplified 2D geometry.

It should be noted that Eq. (2) and consequently Eqs. (3) and (6) are valid for creeping flow regime where the inertial effect of the porous media on the pressure drop is negligible. This assumption is valid when the Reynolds number defined based on the cylinder diameter is less than 8 [30].

To calculate the pressure drop from either Eq. (3) or Eq. (6), one needs to know the permeability. Depending upon the microstructure, the permeability should be calculated from suitable relationships/models; see for example [30–33]. Models that do not take into account the microstructural parameters such as cylinders arrangement and orientations have limited range of applicability that can significantly change the accuracy of Eq. (3) or Eq. (6). The permeability of square arrangement of fibers in the normal directions which is the focus of the current study is discussed in the following subsection.

The relative difference of the predicted values of pressure drop calculated from a 3D analysis, Eq. (3), or a 2D model, Eq. (6), is shown in Fig. 3. It can be seen that the maximum relative difference between the two models for the range of samples with small cross-sectional aspect ratio is less than 8%. Therefore, Eq. (6) can be used for predicting the pressure drop.

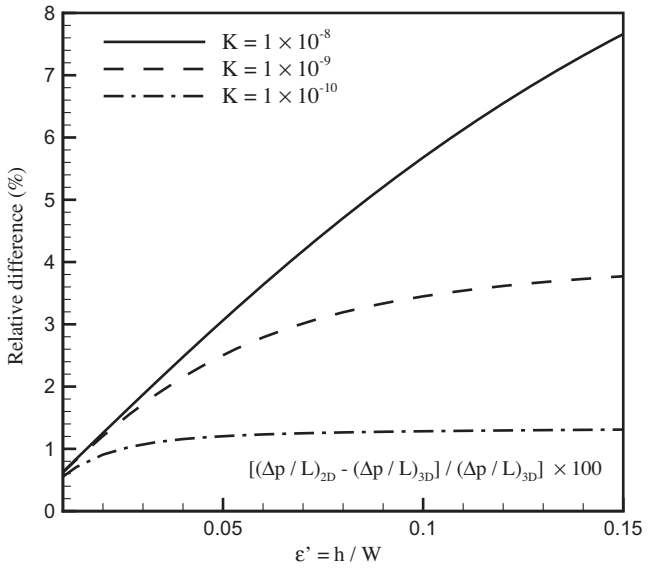

Fig. 3. Relative difference between predicted values of pressure drop based on 3D analysis using Eq. (3), $(\Delta p/L)_{3D}$, and the 2D model presented by Eq. (6), $(\Delta p/L)_{2D}$.

2.1. Permeability of the array of cylinders

The normal permeability of ordered cylinders has been studied extensively in the literature [22,34–37]. Recently, Tamayol and Bahrami [22] have employed an integral technique solution to develop analytical models for permeability of square arrangement of fibers. The porosity (ε) for these arrangements is determined from:

$$\varepsilon = 1 - \frac{\pi d^2}{4S^2} \tag{7}$$

where s is the distance between adjacent cylinders and d is the diameter of the cylinders, as shown in Fig. 1. The following relationship was reported for the permeability of square arrangement of fibers [22]:

$$K^* = \left\{ \frac{12(\sqrt{\varphi'}-1)}{\varphi'\sqrt{\varphi'}}\left[\frac{2-g(\varepsilon)}{2}\right] + \frac{18+12(\varphi'-1)}{\sqrt{\varphi'}(1-\varphi')^2} + \frac{18\sqrt{\varphi'}\left[\tan^{-1}\left(\frac{1}{\sqrt{\varphi'-1}}\right)+\frac{\pi}{2}\right]}{(\varphi'-1)^{\frac{5}{2}}} \right\}^{-1} \tag{8}$$

where $K^* = K/d^2$, $g(\varepsilon) = 1.274\varepsilon - 0.274$, and $\varphi' = \pi/4(1-\varepsilon)$. In Ref. [22], Eq. (8) was successfully verified with experimental data collected from several sources. In this study, Eq. (8) is used to calculate the permeability of the cylinders located inside the microchannels.

3. Experimental procedure

3.1. Microfabrication

Five different PDMS/PDMS samples were fabricated using the soft lithography technique [38] described by Erickson et al. [39]. The fabrication process has two main parts: (1) preparing the mold; (2) making the PDMS replica.

SU-8 is a negative tone, epoxy type, near UV (365 nm) photopatternable material that can be employed as a master for PDMS micromolding. It consists of a polymeric epoxy resin (Epon SU-8) in an organic solvent (gamma Butyrolactone (GBL)) and a photoacid generator taken from the family of the triarylium-sulfonium salts. SU-8-100 was chosen for micromold fabrication as it can be patterned in very thick films (up to 2 mm thick) and makes an excellent mold for PDMS. Square glass slides of 75 × 75 mm and 1 mm thick were used as substrates which were first cleaned in 100% Micro 90 Detergent (purchased from International Products Corporation, USA) using ultrasonic agitation for 5 min and then rinsed with de-ionized (DI) water, acetone, isopropyl alcohol (IPA) and DI water. Substrates were blow dried using nitrogen followed by dehydration baking for 20 min at 120 °C in a convection oven and cooling to room temperature. A 25 nm thick chrome layer was sputtered on each glass substrate which acts as an adhesion promoter for the SU-8 100. A 100 μm thick layer of SU-8 100 was spin coated (at 2250 RPM) on top of the adhesion layer of each substrate, followed by soft baking at 90 °C for 80 min and cooling to room temperature. Structures were patterned using photolithographic UV exposure through a photomask for 60 s. Full crosslinking of the SU-8 100 was achieved by a post-exposure bake at a temperature of 60 °C for 65 min (ramp rate: 300 °C/h) followed by cooling to room temperature.

The structural layer on each substrate was then developed in SU-8 Developer (Microchem™) for 90 s in an ultrasonic bath. Liquid PDMS was then poured over the mold and trapped bubbles were extracted by placing the liquid PDMS inside a vacuum chamber for 1 h. The replica was then cured at 85 °C for 45 min yielding a negative cast of the microchannel pattern. An enclosed microchannel was then formed by bonding the PDMS cast with another piece of PDMS via plasma treatment. The fabrication process is also shown in Fig. 4.

As a result of the fabrication uncertainty, the sizes of the channels and the cylinders were different from their intended dimensions. To measure the actual sizes, an image processing technique, utilized by Akbari et al. [40], was used. Accuracy of this method was reported by Akbari et al. [40] to be ±3.6 μm.

Our images reveal that the surfaces of the fabricated cylinders were rough (see Fig. 5). As such, for determining the cylinders sizes, diameters of several cylinders were measured in three different directions for each sample and the average of these values was considered as the size of the cylinders. In order to measure the width and the depth, the samples were cut at three random locations. The cutting lines were perpendicular to the channel to ensure a 90 deg viewing angle. The average of the measured values was considered as the actual size of the channels. The geometrical properties of the samples are summarized in Table 1. The channels' names in the table indicate the cylinder arrangement, intended porosity, and the expected cylinders diameter, e.g., Sq-0.40-400 corresponds to square arrangement of 400 μm cylinders with a porosity of 0.4. In addition, the permeabilities of the embedded porous media, calculated from Eq. (8), are reported in Table 1.

3.2. Test setup

The open loop system, illustrated in Fig. 6, was employed for measuring the steady pressure drop in the fabricated samples. A syringe pump (Harvard Apparatus, QC, Canada) was employed to provide a user-specified flow rate to the system with a controlled flow rate of 0.5% accuracy. Distilled water was flowed through a submicron filter before entering the channel. To measure the pressure drop, a gauge pressure transducer (Omega Inc., Laval, QC, Canada) was fixed at the channel inlet while the channel outlet was discharged to the atmosphere. Teflon tubing (Scientific Products and Equipment, North York, Canada) was employed to connect the pressure transducer to the syringe pump and the microchannel. Pressure drops were measured for several flow rates in the range of 50–800 μl/min (8.3–103 × 10^{-10} m^3/s).

3.3. Analysis of experimental data

The viscous dissipation effect is neglected in this study; thus, the properties of the flowing water are considered to be constant. The measured pressure drop during the experiment, ΔP_{total}, is:

$$\Delta P_{total} = \Delta P_c + \Delta P_D + \Delta P_{FD} + \Delta P_{\text{minor}} + \Delta P_{ev} \tag{9}$$

where ΔP_c is the pressure loss in the connecting tubes between the pressure transducer and the sample inlet (see Fig. 6), ΔP_D is the pressure drop in the developing region of the samples where the fully-developed flow is not achieved, ΔP_{FD} is the pressure drop in the regions with fully-developed velocity distribution. ΔP_{minor} is the pressure drop due to minor losses in the samples including 90 deg bends in the inlet and outlet of the samples, and ΔP_{ev} is the pressure drop corresponds to the electroviscous effect [41]. Akbari et al. [40] showed that ΔP_{minor} and ΔP_{ev} are less than%1 of the ΔP_{FD}, thus can be neglected.

The connecting pressure loss, ΔP_c, is measured directly at each flow rate when the end of the tubing is disconnected from the sample. To perform accurate measurements, the level of the tubing end should be identical to the case where the samples are connected; this prevents any error due to hydrostatic pressure difference. Akbari et al. [40] showed that the developing pressure drop in microchannels is less than 1% of the total pressure loss and is negligible. In addition, for the case of pack fibers, fully-developed condition is

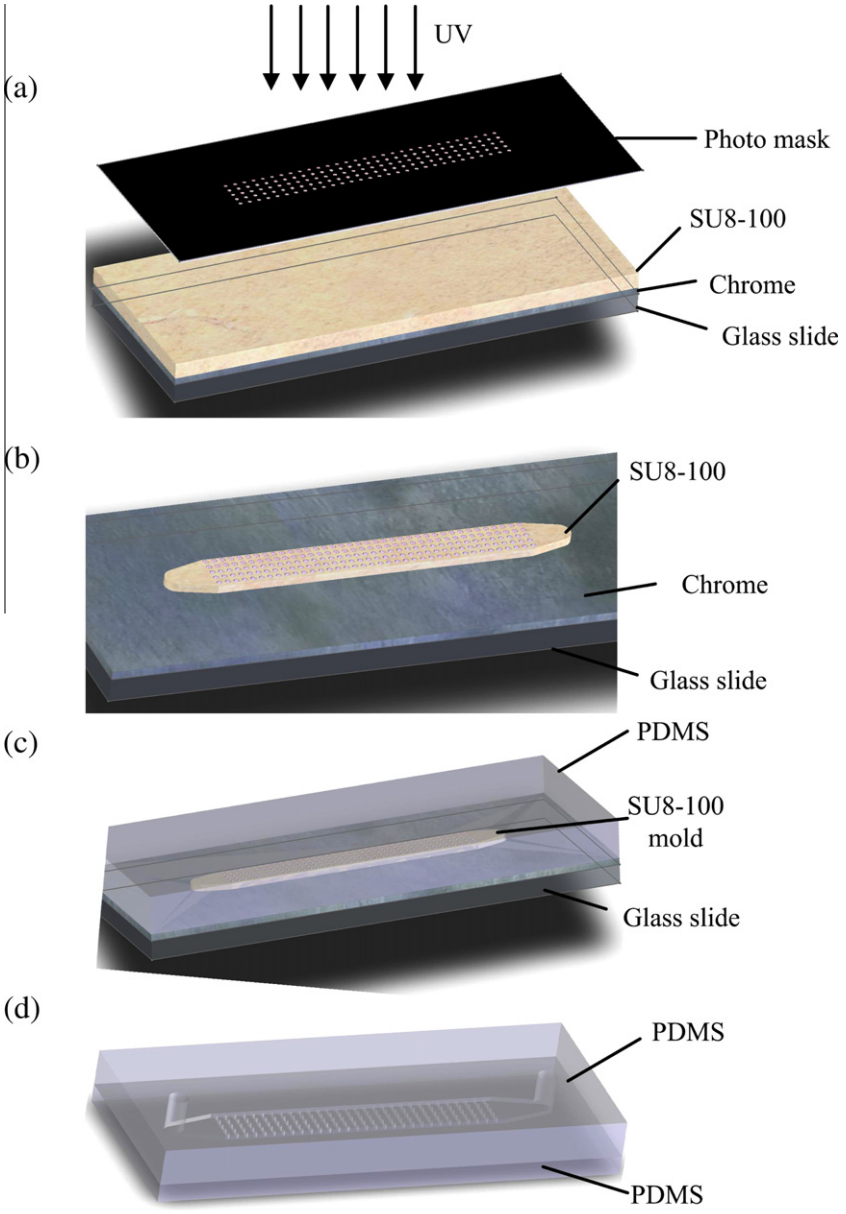

Fig. 4. Fabrication process steps for SU-8 micromold preparation via photopatterning of SU-8 100 epoxy-based photopolymer: (a) UV exposure, (b) making the mold, (c) pouring liquid PDMS, and (d) plasma bonding and making the channels.

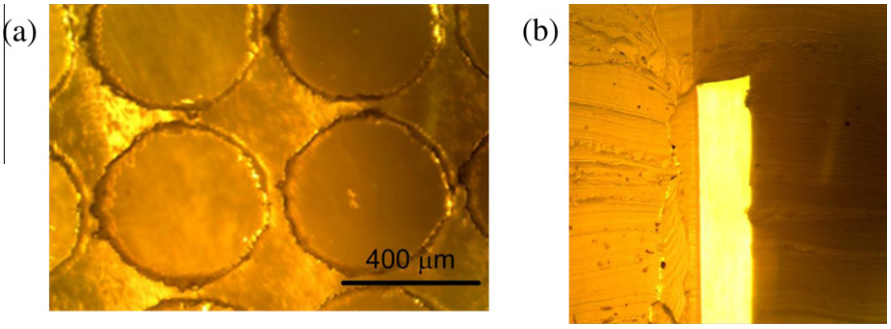

Fig. 5. (a) Rough surface of the fabricated cylinders, Sq-0.4-400 (1), (b) microscope image of the cross-section of Sq-0.95-50.

achieved in the first three rows [42]. Therefore, it is expected that the measured pressure drop in the sample is associated with the fully-developed condition which is presented by Eq. (6).

The uncertainty of the analysis is mostly a result of the uncertainty in the fabrication process and the uncertainty in the channel and cylinder size measurements. These uncertainties will affect the

Table 1
Geometrical properties of the fabricated samples.

Channel	d (μm)	S (μm)	ε	K (m^2), Eq. (8)	W (mm)	h (μm)	L (cm)
Sq-0.40-400 (1)	426	456	0.32	1.85×10^{-11}	3.18	96	1.46
Sq-0.40-400 (2)	418	456	0.34	3.30×10^{-11}	3.19	105	1.46
Sq-0.70-100	92	162.1	0.75	3.93×10^{-10}	1.45	105	1.72
Sq-0.90-50	52	129	0.89	6.89×10^{-10}	1.27	129	2.00
Sq-0.95-50	54	118	0.94	2.49×10^{-9}	1.70	118	2.22

K is for infinitely long equally-sized, equally-spaced cylinders with the reported arrangement.

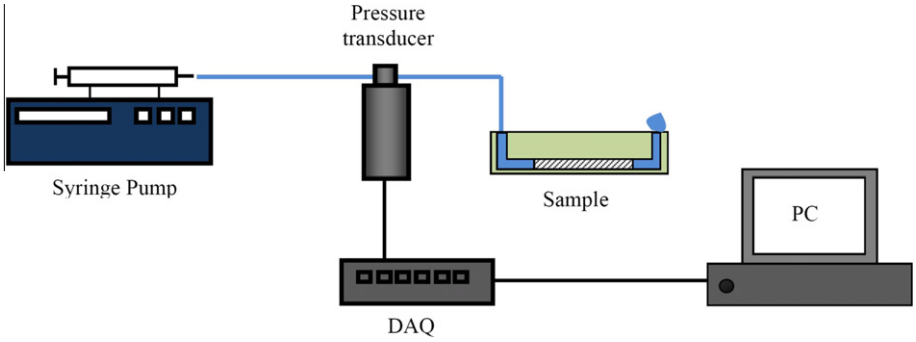

Fig. 6. Schematic of the experimental setup for measuring pressure drop in the tested samples.

porosity and consequently the permeability of the porous medium which is a nonlinear function of porosity. The uncertainty in the permeability predictions can be determined from the following relationship [43]:

$$E(K) = \sqrt{\left(\frac{d(K)}{d(\varepsilon)}E(\varepsilon)\right)^2 + \left(\frac{d(K)}{d(d)}E(d)\right)^2} \tag{10}$$

where $E(\cdot)$ indicated the uncertainty associated with the involved parameters. The uncertainty in the measurement of pressure drop can be evaluated from the following equation:

$$E\left(\frac{\Delta P}{L}\right) = \sqrt{\left(\frac{d(\Delta P/L)}{d(Da)}E(Da)\right)^2 + \left(\frac{d(\Delta P/L)}{d(h)}E(h)\right)^2 + \left(\frac{d(\Delta P/L)}{d(K)}E(K)\right)^2 + \left(\frac{d(\Delta P/L)}{d(Q)}E(Q)\right)^2} \tag{11}$$

where,

$$\frac{E(Da)}{Da} = \sqrt{\left(2\frac{E(h)}{h}\right)^2 + \left(\frac{E(K)}{K}\right)^2} \tag{12}$$

The associated uncertainties with different parameters involved in the analysis are listed in Table 2. It should be noted that despite a small measurements and fabrication uncertainties the overall uncertainty in the pressure drop prediction is significant. This is a direct result of the nonlinear nature of the relationship between geometrical parameters with permeability and the overall pressure drop.

Table 2
Uncertainty in the calculation of the involved parameters.

Sample	$\frac{E(\varepsilon)}{\varepsilon}$	$\frac{E(K)}{K}$	$\frac{E(h)}{h}$	$\frac{E(\Delta p/L)}{\Delta p/L}$
Sq-0.40-400 (1)	0.02	0.59	0.10	0.60
Sq-0.40-400 (2)	0.02	0.54	0.10	0.55
Sq-0.70-100	0.026	0.34	0.10	0.36
Sq-0.90-50	0.02	0.44	0.08	0.44
Sq-0.95-50	0.01	0.07	0.08	0.11

4. Numerical simulations

Our analysis showed a significant uncertainty in the experimental study. Therefore, to further investigate the accuracy of the current analysis, the proposed analytical model, Eqs. (6) and (8), is verified through comparison with the results of numerical simulation of flow (Navier-Stokes equations) through the studied geometries. As such, flow through the geometries listed in Table 1 is solved numerically using Fluent software [44].

Consistent with the analytical approach described in Section 2, the flow is assumed to be fully developed, creeping, and constant properties; therefore, modeling the region between two adjacent cylinders and applying a periodic boundary condition enable us to estimate the pressure gradient in the samples. An example of the considered geometry and the numerical grid produced by Gambit [44] is shown in Fig. 7.

The volumetric flow rate is set in the range covered by the experimental data to ensure that the Reynolds number based on averaged velocity and the cylinders diameter is low and the inertial effects are negligible. Fluent software [44] is used as the solver, which is a finite volume based software. Second order upwind scheme is selected to discretize the governing equations. SIMPLE algorithm is employed for pressure-velocity coupling. The inlet and outlet faces of the geometry are considered to be Periodic. Symmetry boundary condition is applied at sides of the considered unit cell. Grid independency of the solutions is checked to ensure that the predicted pressure drops are independent of the computational grid and numerical grids in the range of 23,000 to 80,000 have been used for conducting numerical simulations.

5. Comparison of the model with the experimental and numerical data

Figs. 8 and 9 include the experimental and numerical values of pressure drop in the tested samples versus the volumetric flow rate. The flow rates were selected such that the pressure drop in the channels was higher than the accuracy of the pressure transducer, i.e., 200 *Pa*. It can be seen that the trends of the experimental data were well predicted by the theoretical results, Eq. (6). The

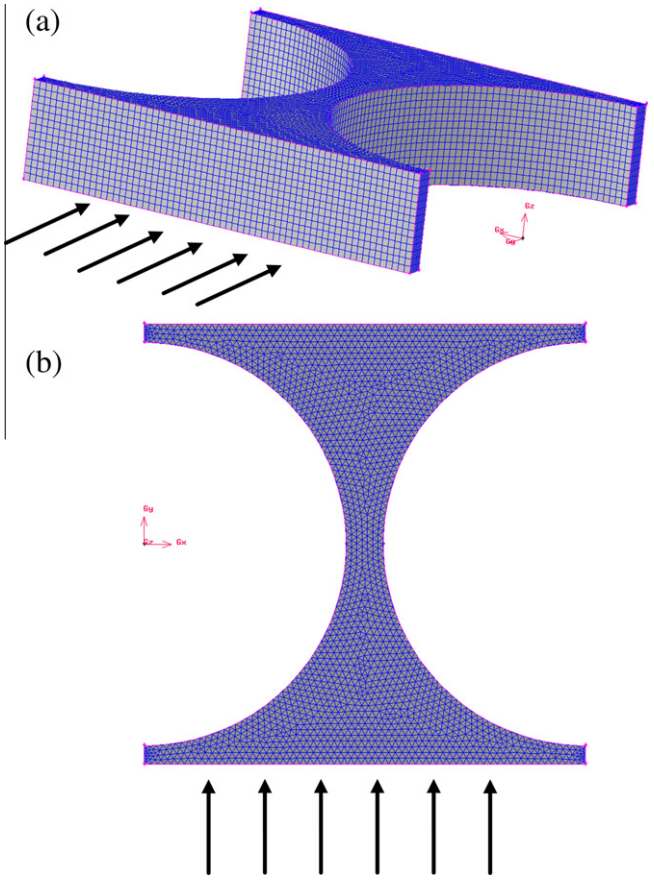

Fig. 7. The considered unit cell between two adjacent cylinders and produced numerical grid for modeling of sample Sq-04-400(2); (a) isometric, (b) top view.

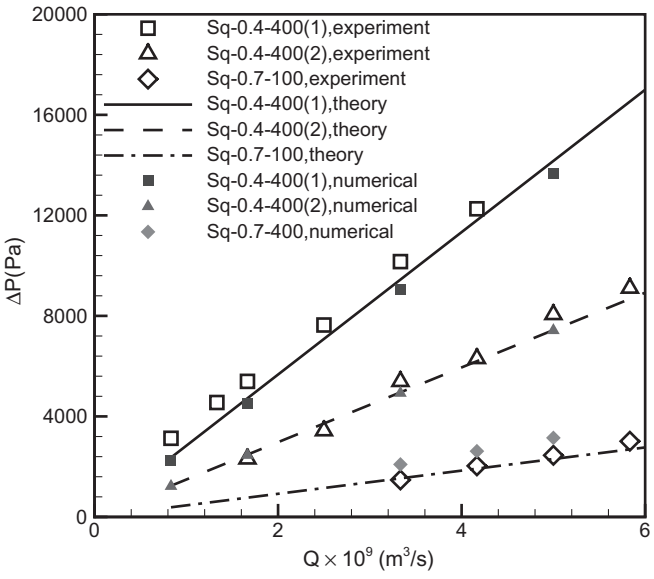

Fig. 8. Channel pressure drop versus flow rate for Sq-0.4-400 (1), Sq-0.4-400 (2), and Sq-0.7-100. Lines show the theoretical values of pressure drop predicted by Eq. (6), hollow symbols show the experimental data, and filled symbols show the numerical results. The channels' names in the table indicate the cylinder arrangement, intended porosity, and the expected cylinders diameter.

difference between most of the measured data and the predicted values from Eq. (6) was less than 15%. The deviations were more intense for Sq-0.9-50 (max 20%); therefore, the ±15% region for

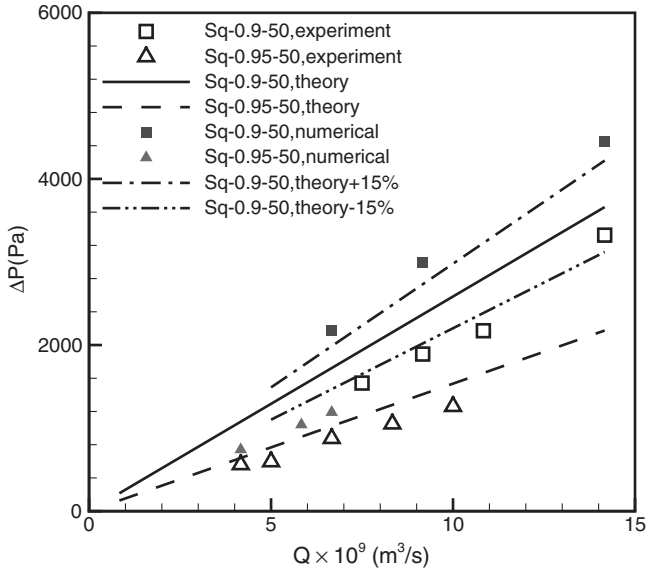

Fig. 9. Experimental, numerical, and theoretical values of channel pressure drop versus flow rate for Sq-0.9-50 and Sq-0.95-50. Lines show the theoretical values of pressure drop predicted by Eq. (6), hollow symbols show the experimental data, and filled symbols show the numerical results. The channels' names in the table indicate the cylinder arrangement, intended porosity, and the expected cylinders diameter.

theoretical predictions is shown in Fig. 9. It should be noted the deviation of the experimental data from the theoretical predictions is mostly caused by the inaccuracy in the channels cross-section measurement as discussed before and the deviations are lower than the uncertainty of the analysis.

The experimental values of pressure drop had a linear relationship with volumetric flow rate. It can be argued that the channels had not been deformed (bulged) during the experiment else a nonlinear trend would have been observed in the experimental data; for detailed discussions see [45]. Moreover, the linear trend of the experimental data shows that the minor losses and the inertial effects are insignificant in the tested samples. It should be noted that the maximum Reynolds number based on cylinders' diameter is less than 5; this justifies the observed trends in the measured values.

A comparison between the values obtained for pressure drop in sample Sq-0.40-400 (1) and Sq-0.40-400 (2) shows that a small variation of porosity (±0.02) has resulted in a variation of the pressure drop by 50%. This clearly indicates the impact of the geometrical parameters on the resulting pressure drop and shows that the deviation between the simple model with the numerical and experimental data is reasonable within the context of porous media. Moreover, it can be concluded that the proposed approach, despite its simplicity in comparison with other existing solutions in the literature, is practical and can be employed in the design process of microfluidic systems.

6. Effect of various parameters

In the studied porous-filled microchannels, two parameters affect the pressure drop the most: (1) the permeability, K; (2) the channel depth, h. To investigate the effect of these parameters, the dimensionless pressure drop is plotted versus the Darcy number (K/h^2) in Fig. 10. It can be seen that Eq. (6) is in reasonable agreement with the experimental data. In addition, two asymptotes can be recognized in Eq. (6): (1) Darcy and (2) Stokes flow asymptotes.

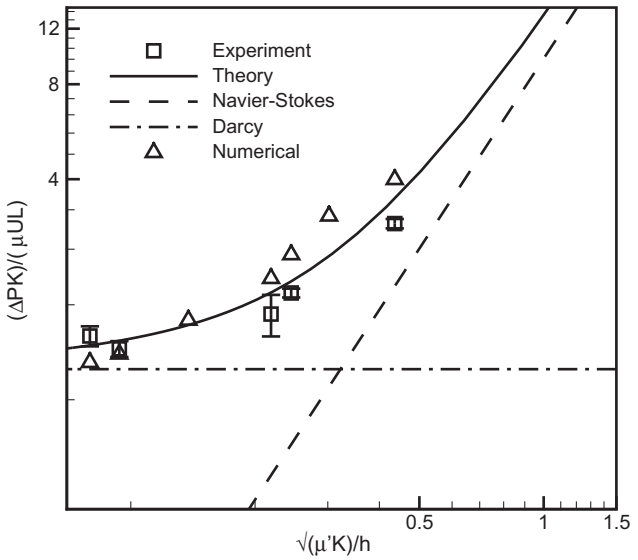

Fig. 10. Dimensionless pressure drop versus Darcy number.

For structures with very dilute porous medium, low Darcy number, the pressure drop can be predicted by solving the Stokes equations for plain fluid. For channels with very packed porous medium, high Darcy numbers, Eq. (6) and the Darcy law predict the same results. As such, one can conclude that the Darcy number can be used for determining the controlling parameter in the pressure drop.

Fig. 10 shows whether the wall effects should be considered in the analysis of problems that include convective transport phenomena through porous-filled microchannels. For example, in experiments with the goal to determine the transport properties of new micro/nano structures, Fig. 10 can be employed to determine the minimum channel dimensions that have an insignificant effect on the predicted results.

7. Summary and conclusions

Pressure drop in microchannels filled with a porous structure comprised of straight cylinders in ordered arrangements was studied. The Brinkman equation was used to predict the overall pressure drop. The permeability of the porous medium in the volume averaged equations was evaluated from the model proposed by [22] for the permeability of square arrangement of fibers.

The soft lithography method was employed to fabricate five PDMS samples with porosity in the range of 0.33 to 0.95, fiber diameter from 50 to 400 μm, approximately 100 μm deep. Water was flowed through the samples via pressure-driven flow provided by syringe pump and the overall pressure drop was measured for different flow rates. Moreover, to verify the theoretical analysis, flow through the fabricated structures was numerically solved and the values of pressure drop were determined. The theoretical model was successfully compared with the numerical and experimental data. Our analysis suggested that the Darcy number was the suitable dimensionless number for determining the controlling parameter over the pressure drop. For high Darcy numbers, the channel dimensions played a major role in the overall pressure drop while in low Darcy numbers the cylinders geometry and permeability were the controlling parameters in determining the pressure drop.

It should be noted that the proposed approach is applicable for analyzing flow through other types of porous media embedded in mini/microchannels.

Acknowledgements

The authors gratefully acknowledge the financial support of the Natural Sciences and Engineering Research Council of Canada (NSERC). A.T. thanks British Columbia Innovation Council (BCIC) financial support.

References

[1] A.I. Gunther, S.A. Khan, M. Thalmann, F. Trachsel, K.F. Jensen, Transport and reaction in microscale segmented gas-liquid flow, Lab Chip 4 (4) (2004) 278–286.
[2] S.W. Cha, R. O'Hayre, F.B. Prinz, The influence of size scale on the performance of fuel cells, Solid State Ionics 175 (1–4) (2004) 789–795.
[3] J.C. Harley, Y. Huang, H.H. Bau, J.N. Zemel, Gas flow in micro-channels, J. Fluid Mech. 284 (1995) 257–274.
[4] J. De Jong, M.J. Geerken, R.G.H. Lammertink, M. Wessling, Porous microfluidic devices – fabrication and applications, Chem. Eng. Technol. 30 (3) (2007) 309–315.
[5] C.S. Effenhauser, A. Manz, H.M. Widmer, Glass chips for high-speed capillary electrophoresis separations with submicrometer plate heights, Anal. Chem. 65 (19) (1993) 2637–2642.
[6] L. Tadrist, M. Miscevic, O. Rahli, F. Topin, About the use of fibrous materials in compact heat exchangers, Exp. Thermal Fluid Sci. 28 (2–3) (2004) 193–199.
[7] P.R. Waghmare, S.K. Mithra, A. Mather, J. McLaughlin, Modeling, fabrication and simulation of microfilters, in: ECI International Conference on Heat Transfer and Fluid Flow in Microscale, Whistler, Canada, 2008.
[8] T. Yamada, C. Hong, O. Gregory, M. Faghri, Experimental investigations of liquid flow in rib-patterned microchannels with different surface wettability, Microfluid. Nanofluid. (2011) 1–11.
[9] S. Khirevich, A. Höltzel, D. Hlushkou, U. Tallarek, Impact of conduit geometry and bed porosity on flow and dispersion in noncylindrical sphere packings, Anal. Chem. 79 (24) (2007) 9340–9349.
[10] C. Yu, M.H. Davey, F. Svec, J.M.J. Fréchet, Monolithic porous polymer for on-chip solid-phase extraction and preconcentration prepared by photoinitiated in situ polymerization within a microfluidic device, Anal. Chem. 73 (21) (2001) 5088–5096.
[11] D.J. Throckmorton, T.J. Shepodd, A.K. Singh, Electrochromatography in microchips: reversed-phase separation of peptides and amino acids using photopatterned rigid polymer monoliths, Anal. Chem. 74 (4) (2002) 784–789.
[12] A. Haji-Sheikh, Fully developed heat transfer to fluid flow in rectangular passages filled with porous materials, J. Heat Transfer 128 (6) (2006) 550–556.
[13] A. Haji-Sheikh, W.J. Minkowycz, E.M. Sparrow, Green's function solution of temperature field for flow in porous passages, Int. J. Heat Mass Transf. 47 (22) (2004) 4685–4695.
[14] A.V. Kuznetsov, M. Xiong, D.A. Nield, Thermally developing forced convection in a porous medium: circular duct with walls at constant temperature, with longitudinal conduction and viscous dissipation effects, Transp. Porous Media 53 (3) (2003) 331–345.
[15] K. Hooman, A superposition approach to study slip-flow forced convection in straight microchannels of uniform but arbitrary cross-section, Int. J. Heat Mass Transf. 51 (15–16) (2008) 3753–3762.
[16] K. Hooman, Slip flow forced convection in a microporous duct of rectangular cross-section, Appl. Therm. Eng. 29 (5–6) (2009) 1012–1019.
[17] N. Scales, R.N. Tait, Modeling electroosmotic and pressure-driven flows in porous microfluidic devices: Zeta potential and porosity changes near the channel walls, J. Chem. Phys. 125 (9) (2006) 094714.
[18] A. Kosar, C. Mishra, Y. Peles, Laminar flow across a bank of low aspect ratio micro pin fins, J. Fluids Eng. 127 (3) (2005) 419–430.
[19] S. Vanapalli, H.J.M. ter Brake, H.V. Jansen, J.F. Burger, H.J. Holland, T.T. Veenstra, M.C. Elwenspoek, Pressure drop of laminar gas flows in a microchannel containing various pillar matrices, J. Micromech. Microeng. 17 (7) (2007) 1381.
[20] J. Yeom, D.D. Agonafer, J.H. Han, M.A. Shannon, Low Reynolds number flow across an array of cylindrical microposts in a microchannel and figure-of-merit analysis of micropost-filled microreactors, J. Micromech. Microeng. 19 (6) (2009) 065025.
[21] G. Gamrat, M. Favre-Marinet, S. Le Person, R. Baviere, F. Ayela, An experimental study and modelling of roughness effects on laminar flow in microchannels, J. Fluid Mech. 594 (2008) 399–423.
[22] A. Tamayol, M. Bahrami, Analytical determination of viscous permeability of fibrous porous media, Int. J. Heat Mass Transf. 52 (9–10) (2009) 2407–2414.
[23] W. Zhong, I. Currie, D. James, Creeping flow through a model fibrous porous medium, Exp. Fluids 40 (1) (2006) 119–126.
[24] H.C. Brinkman, A calculation of the viscous force exerted by a flowing fluid on a dense swarm of particles, Appl. Sci. Res. 1 (1) (1949) 27–34.
[25] R.C. Givler, S.A. Altobelli, A determination of the effective viscosity for the Brinkman–Forchheimer flow model, J. Fluid Mech. 258 (1) (1994) 355–370.
[26] A. Tamayol, K. Hooman, M. Bahrami, Thermal analysis of flow in a porous medium over a permeable stretching wall, Transp. Porous Media 85 (3) (2010) 661–676.
[27] V.M. Starov, V.G. Zhdanov, Effective viscosity and permeability of porous media, Colloids Surf., A 192 (1–3) (2001) 363–375.

[28] J.A. Ochoa-Tapia, S. Whitaker, Momentum transfer at the boundary between a porous medium and a homogeneous fluid–I, theoretical development, Int. J. Heat Mass Transf. 38 (14) (1995) 2635–2646.
[29] K. Hooman, A.A. Merrikh, Analytical solution of forced convection in a duct of rectangular cross section saturated by a porous medium, J. Heat Transfer 128 (6) (2006) 596–600.
[30] M.M. Tomadakis, T.J. Robertson, Viscous permeability of random fiber structures: comparison of electrical and diffusional estimates with experimental and analytical results, J. Compos. Mater. 39 (2) (2005) 163–188.
[31] M. Kaviany, Principles of Heat Transfer in Porous Media, second ed., Springer-Verlag, New York, 1995.
[32] B.T. Astrom, R.B. Pipes, S.G. Advani, On flow through aligned fiber beds and its application to composites processing, J. Compos. Mater. 26 (9) (1992) 1351–1373.
[33] A. Tamayol, M. Bahrami, In-plane gas permeability of proton exchange membrane fuel cell gas diffusion layers, J. Power Sources 196 (7) (2011) 3559–3564.
[34] M. Sahraoui, M. Kaviany, Slip and no-slip velocity boundary conditions at interface of porous, plain media, Int. J. Heat Mass Transf. 35 (4) (1992) 927–943.
[35] J. Happel, Viscous flow relative to arrays of cylinders, AIChE J. 5 (2) (1959) 174–177.
[36] A. Tamayol, M. Bahrami, Transverse permeability of fibrous porous media, Phys. Rev. E 84 (4) (2011) 046314.
[37] J.P.D. Plessis, Analytical quantification of coefficients in the Ergun equation for fluid friction in a packed bed, Transp. Porous Media 16 (2) (1994) 189–207.
[38] J.C. McDonald, D.C. Duffy, J.R. Anderson, D.T. Chiu, H. Wu, O.J.A. Schueller, G.M. Whitesides, Fabrication of microfluidic systems in poly(dimethylsiloxane), Electrophoresis 21 (1) (2000) 27–40.
[39] D. Erickson, D. Sinton, D. Li, Joule heating and heat transfer in poly(dimethylsiloxane) microfluidic systems, Lab Chip 3 (2003) 141–149.
[40] M. Akbari, D. Sinton, M. Bahrami, Pressure drop in rectangular microchannels as compared with theory based on arbitrary cross section, J. Fluids Eng. 131 (4) (2009). 041202-041201-041208.
[41] R.F. Probstein, Physicochemical hydrodynamics: an introduction, second ed., John Wiley & Sons Inc., New York, 1994.
[42] A.A. Kirsch, N.A. Fuchs, Studies on fibrous aerosol filters–II. pressure drops in systems of parallel cylinders, Ann. Occup. Hyg. 10 (1) (1967) 23–30.
[43] J.R. Taylor, An introduction to error analysis: the study of uncertainties in physical measurements, Second ed, University Science Books, Sausalito, USA, 1997.
[44] Fluent 6.3 User's Guide, Fluent Inc., Lebanon, USA, 2007.
[45] M.A. Holden, S. Kumar, A. Beskok, P.S. Cremer, Microfluidic diffusion diluter: bulging of PDMS Microchannels under pressure driven flow, J. Micromech. Microeng. 13 (2003) 412–418.